Water Research 266 (2024) 122335

Contents lists available at ScienceDirect

Water Research

journal homepage: www.elsevier.com/locate/watres

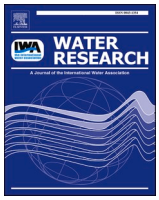

Revisiting the chloramination of phenolic compounds: Formation of novel high-molecular-weight nitrogenous disinfection byproducts

Pin Wang [a], Bei Ye [a,c], Youhei Nomura [a,b], Taku Fujiwara [a,b,*]

[a] Department of Environmental Engineering, Graduate School of Engineering, Kyoto University, Kyoto-Daigaku-Katsura, Nishikyo-ku, Kyoto 615-8540, Japan
[b] Department of Global Ecology, Graduate School of Global Environmental Studies, Kyoto University, Kyoto-Daigaku-Katsura, Nishikyo-ku, Kyoto 615-8540, Japan
[c] Key Laboratory of Microorganism Application and Risk Control of Shenzhen, Guangdong Provincial Engineering Research Center for Urban Water Recycling and Environmental Safety, Shenzhen International Graduate School, Tsinghua University, Shenzhen 518055, PR China

ARTICLE INFO

Keywords:
Phenolic compounds
Chloramination
Nitrogenous disinfection byproducts
Density functional theory calculation
Reaction mechanism

ABSTRACT

Disinfection is critical for ensuring water safety; however, the potential risks posed by disinfection byproducts (DBPs) have raised public concern. Previous studies have largely focused on low-molecular-weight DBPs with one or two carbon atoms, leaving the formation of high-molecular-weight DBPs (HMW DBPs, with more than two carbon atoms) less understood. This study explores the formation of HMW DBPs during the chloramination of phenolic compounds using a novel approach that combines high-resolution mass spectrometry with density functional theory (DFT) calculations. For the first time, we identified nearly 100 previously unreported HMW nitrogenous DBPs (N-DBPs), with nearly half of those being halogenated N-DBPs. These N-DBPs were tentatively identified as heterocyclic (e.g., pyrrole and pyridine analogs) and coupling heterocyclic N-DBPs. Through detailed structure analysis and DFT calculations, the key formation steps of heterocyclic N-DBPs (monochloramine-mediated ring-opening reactions of halobenzoquinones) and new bonding mechanisms (C–N, C–O, and C–C bonding) of the coupling heterocyclic N-DBPs were elucidated. The selective formation of these novel N-DBPs was significantly influenced by factors such as contact time, monochloramine dosage, pH, and bromide concentration. Our findings emphasize the occurrence of diverse HMW heterocyclic N-DBPs, which are likely toxicologically significant, underscoring the need for further research to evaluate and mitigate their potential health risks in water disinfection.

1. Introduction

Water disinfection is critical for public health, yet it comes with the unintended consequence of forming disinfection by-products (DBPs) through reactions between disinfectants and organic or inorganic components in the water. Over 800 DBPs have been identified, most of which are primarily low-molecular-weight (LMW, C_1 to C_2), such as haloacetaldehydes and haloacetonitriles (Chen et al., 2023; Li and Mitch, 2018; Plewa et al., 2010; Richardson and Ternes, 2018). However, regulated LMW DBPs (e.g., trihalomethanes and haloacetic acids) (~0.2 %) and unregulated LMW DBPs (~16 %) together account for only ~17 % of the total cytotoxicity, leaving ~83 % of the total cytotoxicity drivers uncharacterized, suggesting the presence of unknown toxic DBPs (Lau et al., 2023). This uncharacterized fraction, believed to be dominated by higher-molecular-weight DBPs (HMW, $>C_2$) (Mitch et al., 2023), is poorly understood but potentially more toxic.

Recent studies have begun to uncover these HMW DBPs. Pan et al. reported several halogenated DBPs formed in chlorinated water, including halophenols and halosalicylic acids (Pan et al., 2017; Pan and Zhang, 2013; Yang and Zhang, 2013; Zhai and Zhang, 2011). Li et al. reported the formation of 15 haloaromatic DBPs during chlorination of tea water (Li et al., 2021). Additionally, during chlorination, twenty-six novel halogenated DBPs have been identified from tannic acid and its biodegradation products, including DBPs with six-membered ring, five-membered ring, and aliphatic compounds (Yang et al., 2019). Other studies have reported HMW DBPs like halogenated benzoquinones (Hu et al., 2022; Wang et al., 2013), halogenated benzonitriles (Zhang et al., 2021; Zhang et al., 2018), halogenated anilines (Sun et al., 2024; Zhang et al., 2022), and coupling DBPs (Li et al., 2022; Wendel et al., 2014; Xiang et al., 2020). However, these identified compounds represent only a fraction of the HMW DBP fraction, leaving a substantial portion of this category unexplored (Mitch et al., 2023). Identifying these HMW DBPs,

* Corresponding author.
E-mail address: fujiwara.taku.3v@kyoto-u.ac.jp (T. Fujiwara).

https://doi.org/10.1016/j.watres.2024.122335
Received 20 June 2024; Received in revised form 23 August 2024; Accepted 24 August 2024
Available online 26 August 2024

particularly those with significant toxicological implications, such as nitrogenous disinfection by-products (N-DBPs), is crucial due to their potential health risks.

N-DBPs are especially concerning because they exhibit significantly higher genotoxicity, cytotoxicity, and carcinogenicity compared to many carbonaceous DBPs (C-DBPs) (Muellner et al., 2007; Plewa et al., 2008, 2004; Shah and Mitch, 2012). N-DBPs primarily form through two pathways: the reaction of nitrogen-containing organic precursors (e.g., amino acids) (Hoigné and Bader, 1988; Joo and Mitch, 2007; Tang et al., 2021; Zhou et al., 2023), or the incorporation of inorganic nitrogen into dissolved organic matter (Nihemaiti et al., 2017), such as chloramine-nitrogen incorporation. Chloramines, primarily monochloramine (NH_2Cl), are commonly used as secondary disinfectants because of their ability to reduce the formation of regulated trihalomethanes and haloacetic acids (Awwa Disinfection Systems Committee, 2008; Kirmeyer, 2004; Seidel et al., 2005). With the increasing reliance on chloramination, identifying novel HMW N-DBPs formed during chloramination has become a crucial area of DBP research. However, most studies have primarily focused on expected products, such as nitro/nitroso DBPs, halogenated benzonitriles, and halogenated anilines as previously mentioned.

High-resolution mass spectrometry (HRMS) is favored for identifying HMW DBPs due to its superior mass accuracy and high resolution. Based on accurate-mass MS and MS^2 spectra, HRMS-based non-target screenings can provide tentative chemical identifications for HMW DBPs without initial standards (Angeles et al., 2021; Dualde et al., 2023; Lu et al., 2021; Nihemaiti et al., 2023; Wang et al., 2018). However, the confidence in these HRMS-based identifications varies between studies and substances, necessitating complementary methods. Advances in quantum chemical computing, particularly density functional theory (DFT), allow for predictions of chemical reactivity, offering insights into reaction pathways and mechanisms (Chen et al., 2024; Pan et al., 2013; Zhang et al., 2020; Zhang et al., 2020). The Intrinsic Reaction Coordinate (IRC) in DFT calculations is a theoretical tool that aids in proposing plausible reaction mechanisms by tracing pathways from reactants to products. This approach is particularly useful when available standards can serve as "positive controls", allowing predictions from IRC calculations to be verified and thereby supporting the identification of unknown products.

Given the complexity of natural organic matter and the poor characterization of HMW DBPs, model precursor compounds offer a simplified approach for initial analyses. The ideal model precursors for analysis of N-DBPs formed via inorganic nitrogen pathways should possess aromatic structures, lack nitrogen atoms, and exhibit good reactivity with chloramines. Phenolic compounds, which are prevalent in both natural organic matter and anthropogenic chemicals, such as plastic pipe additives, are suitable candidates due to their high reactivity with chlorine-based disinfectants (Aeschbacher et al., 2012; Fiss et al., 2007; Li and Mitch, 2018; Prasse et al., 2020; Tentscher et al., 2018). Therefore, we selected both simple phenolic compounds, such as phenol, 4-chlorophenol, and 4-bromophenol, and the more complex polyphenol, bisphenol A (BPA), as model precursors. The main objective of this study is to establish a framework for identifying novel N-DBPs resulting from the chloramination of typical phenolic compounds. By combining HRMS with DFT calculations, we aim to map the reaction pathways leading to novel N-DBPs both theoretically and experimentally. Additionally, we investigate the effects of the reaction conditions and structure on the mechanisms and profiles of these N-DBPs.

2. Materials and methods

2.1. Chemicals

Supporting Information Text S1 provides material sources.

2.2. Chloramination experiments and sample pretreatment

Monochloramine (NH_2Cl) was freshly prepared following an established method: ammonium chloride was dissolved in water adjusted to pH 8.5, and sodium hypochlorite was then titrated into the ammonium chloride solution at an N:Cl molar ratio of 1.2:1 (Schreiber and Mitch, 2005). The concentrations of NH_2Cl and dichloramine ($NHCl_2$) were determined spectrophotometrically at 245 and 295 nm, respectively (Valentine et al., 1986). Chloramination experiments were conducted at $23 \pm 2°C$ in headspace-free amber glass bottles. Model compounds were used at higher concentrations to ensure robust detection and identification of DBPs. To explore the influence of disinfection conditions on DBP formation, chloramination was conducted at different molar ratios of NH_2Cl: precursor (5:1, 10:1, 20:1, and 50:1), pH values (4, 6, 7, 8, 9, and 10), and time intervals (0–48 h). pH values ranging from 6 to 8 were adjusted using 5 mM phosphate buffer, while pH values outside this range were adjusted using either 0.1 M NaOH or H_2SO_4. To evaluate the impact of bromide on the DBPs profile, experiments were performed using concentrations ranging from 5 to 20 μM. Additionally, the effects of adding 3 mg-C/L natural organic matter (NOM) and 2 mM bicarbonate on the formation of N-DBPs were examined. Further experiments were conducted using low concentrations of model compounds, close to environmentally relevant levels, to test N-DBP formation during chloramination. Specifically, 0.1 μM BPA and 0.02 μM simple phenolic compounds were chloraminated by dosing with 1 mg/L NH_2Cl for a 24-hour contact time at pH 7. The solid-phase extraction procedure is detailed in Text S2. NH_2Cl was quenched using a 2-fold molar excess of sodium thiosulfate. All experiments were performed in triplicate.

2.3. Analytical methods

To determine the precise molecular formulas of the novel DBPs, all sample extracts were subjected to chemical and molecular structural characterization using ultra-high-performance liquid chromatography-Orbitrap high-resolution mass spectrometry (UHPLC-Orbitrap HRMS, Q Exactive Focus; Thermo Fisher Scientific, USA). Detailed analysis conditions are provided in Text S3. Given the uncertain structures of the N-DBPs, samples were analyzed in both positive and negative ion modes using electrospray ionization. The MS^1 (recorded with a resolution of 35,000) were acquired with a mass error (Δm) setting within 5 ppm (Jeon et al., 2013), whereas the mass error of the MS^2 (recorded with a resolution of 17,500) were acquired with a Δm within 20 ppm. The MS^2 were obtained through high-energy collisional dissociation (HCD), with energy levels ranging from 20 to 50 eV to obtain fragment ions and neutral losses. Data were analyzed using Compound Discoverer (CD) 3.3. For elemental composition analysis (MS^1), CD was configured with parameters including a signal-to-noise threshold of 3 for peak picking, mass tolerance of 5 ppm, and minimum peak intensity of 10,000 (Lu et al., 2021). Accurate m/z values of the detected peaks were extracted using Xcalibur (with an m/z window of 5 ppm) to confirm their presence. For fragment analysis (MS^2), some MS^2 fragment algorithms provided by Mass Frontier and Fragmentation Ion Search were employed. Unknown compounds were identified by comparing their proposed structures with those generated from fragments, using compound databases such as ChemSpider and PubChem (Yu et al., 2023). In the absence of authentic standards, relative concentrations were represented using peak areas from single-ion monitoring. The concentrations of model compounds were measured using the UPLC system (Waters Corp., Milford, MA, USA), as described in Table S1.

2.4. Computational method

All calculation were conducted using the Gaussian 16 program suite at 298.15 K and 1 atm (Liljenberg et al., 2018; Zhang et al., 2021). Reactants and products were optimized to a stationary point, and frequency analysis was conducted to confirm the absence of an imaginary

frequency. Transition states (TS) were verified by the presence of a single imaginary frequency and its connection to the designated reactants and products in the intrinsic reaction coordinate analysis. For each reaction, Gibbs free energy (ΔG, kcal/mol) was calculated to provide insight into the thermodynamic feasibility of the proposed reaction, while the free energy of activation ($\Delta G^{\ddagger}$) was used to assess kinetic feasibility. The detailed methods are provided in Text S4.

3. Results and discussion

3.1. Formation of novel N-DBPs during chloramination of simple phenolic precursors

Based on previous research indicating the formation of N-DBPs from the chloramination of resorcinol (Nihemaiti et al., 2017), we investigated the chloramination of three simple phenolic model compounds: phenol, 4-chlorophenol, and 4-bromophenol. The reactions were conducted at pH 7 with an NH_2Cl/model compound molar ratio of 10:1. HRMS analysis preliminarily identified nearly 30 novel N-DBPs. Analysis of their MS^2 fragments suggested that these newly formed N-DBPs are likely heterocyclic. To confirm the identity of these N-DBPs, we compared the chromatograms and MS^2 fragments of the samples with those of corresponding standards. As shown in Fig. 1(a–c), the high similarity confirmed that the N-DBPs observed at RT 9.05 min (in phenol and 4-chlorophenol samples) and RT 10.10 min (in 4-bromophenol sample) were 5-chloro-2-hydroxypyridine and 5-bromo-2-hydroxypyridine, respectively. Additionally, N-DBPs with MS^2 fragments nearly identical to those of the standards were identified at RT 9.76 min (in phenol and 4-chlorophenol samples) and RT 10.67 min (in 4-bromophenol sample), suggesting the presence of isomers or tautomeric structures (Fig. S1–S2). Various pyridine derivatives, such as hydroxyl, halogenated, and carboxychloropyridine derivatives, were also identified (Fig. S3–S6). For semi-quantitative analysis, we assumed that N-DBPs without standards exhibit similar instrumental responses to molecules with analogous structures. Although this assumption aids in estimating relative abundance, it may introduce some deviations from actual concentrations. As shown in Fig. 1(d), the concentration of N-DBPs increased continuously over 0-96 hours, reaching up to 35.86 μg/L (phenol sample), 43.46 μg/L (4-chlorophenol), and 89.03 μg/L (4-bromophenol), respectively. This suggests a previously unrecognized ring cleavage and nitrogen incorporation pathway leading to the formation of pyridine and its derivatives. Fig. 1(e–f) compare these N-DBPs with the expected chlorinated products in the phenol and 4-chlorophenol samples. The chlorinated products considered mainly include 4-chlorophenol, 2-chlorophenol, and 2,4-dichlorophenol. It should be noted that our yield calculations are based on the concentration of DBPs relative to the precursor consumed, expressed in μg/L per μM of precursor. As illustrated, the accumulation of chlorinated products decreased over time. Specifically, in the phenol sample, the yield of chlorinated products initially peaked at 35.18 μg/L at 24 hours, but then decreased to 2.13 μg/L by 96 hours. In contrast, the accumulation of N-DBPs steadily increased, with the maximum yield reaching nearly 1 μg/L at 96 hours. This observation suggests that although N-DBPs may not constitute the primary formation pathway, their stability could render them more

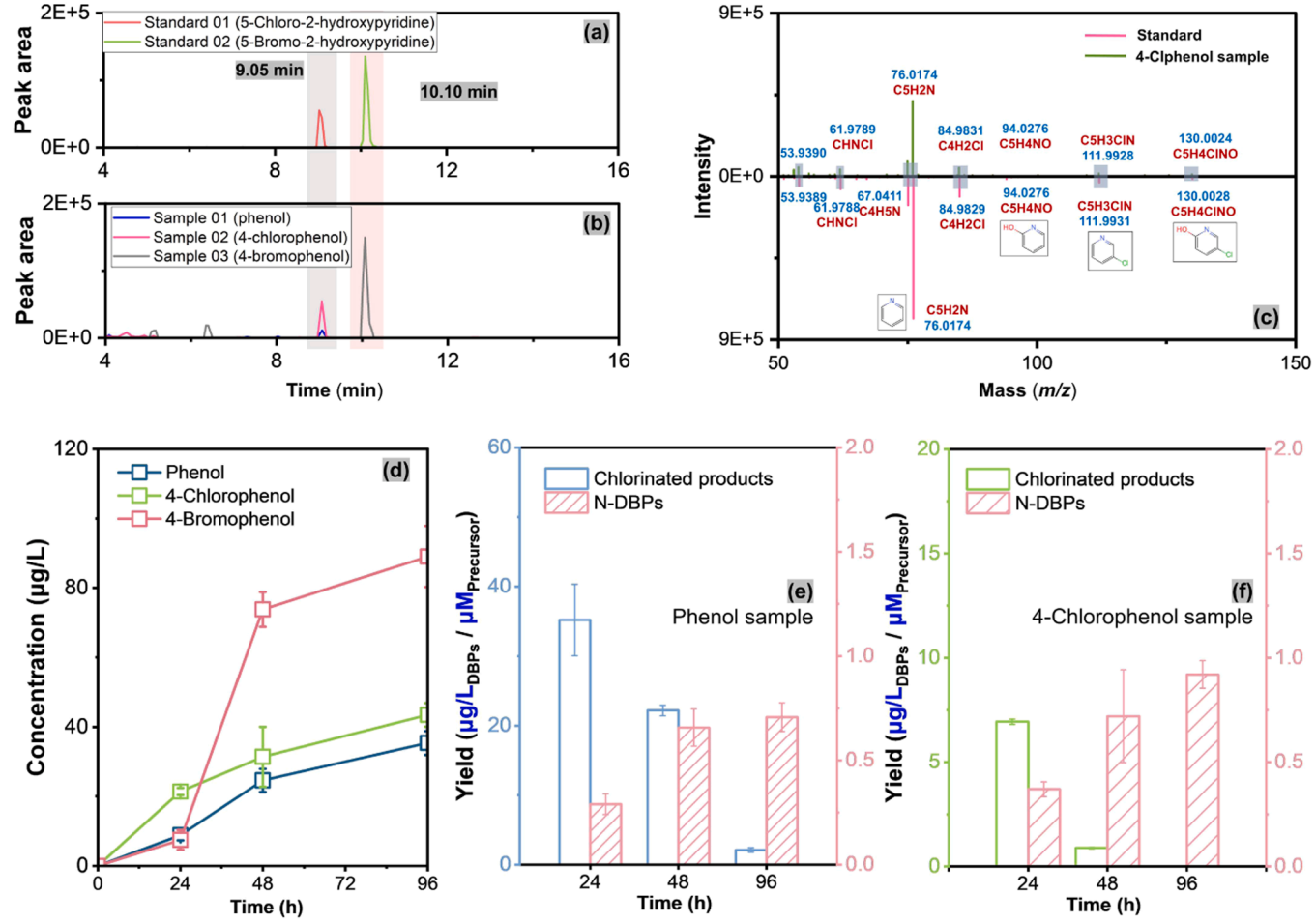

Fig. 1. (a-c) Comparison of chromatograms and MS2 spectra of samples and standards; (d) Concentrations of N-DBPs formed during chloramination of three simple phenolic precursors; (e-f) Comparison of the yields of chlorinated products and N-DBPs. Experimental conditions: [phenolic precursors]0 = 50 μM, [NH2Cl]0 = 500 μM, T = 23 ± 2°C, [phosphate buffer] = 5.0 mM, pH = 7 ± 0.2.

prevalent over extended contact times, potentially leading to their dominance in long-term disinfection scenarios. Additionally, various C4-based N-DBPs, such as *m/z* 177 (pos, exact mass: 179.9499; Δm = 0.5794 ppm, $C_4H_5BrNO_2$). Based on the exact mass obtained from HRMS and the observed MS^2 fragments, consistent with literature data (Nihemaiti et al., 2017) with the same characteristic neutral loss (CO and CONH), we propose that this class of N-DBPs may be pyrrole analogues.

3.2. Quantum chemical validation of formation pathways and structures of novel N-DBPs

We elucidated the formation mechanisms of N-DBPs based on those detected in chloraminated 4-chlorophenol and 4-bromophenol samples (Fig. S7–S8). Our proposed mechanism for heterocyclic N-DBPs relies on two fundamental premises: (1) halogenated benzoquinones (HBQs) serve as crucial intermediates. This hypothesis is supported by previous studies that have identified HBQs as significant intermediates in similar reactions (Kosaka et al., 2017; Yamamoto and Yasuhara, 2002; Zhao et al., 2012), and (2) the conversion rate of HBQ to aliphatic DBP remains below 30 % (based on the conversion rate of elemental carbon), indicating the presence of alternative forms of carbon (Gao et al., 2024). The formation of the carbonyl group (C=O) initiates the sequence, where para-substituted phenolic compounds undergo oxidative transformations to yield C=O, facilitating the formation of ketones such as dichloroquinones. These ketones react with NH_2Cl, where the nitrogen atom undergoes nucleophilic addition to the carbon-oxygen double bond, generating an intermediate. This intermediate undergoes ring-opening, cleaving the carbon-nitrogen bond and generating a reactive intermediate that re-engages with nitrogen, forming a new

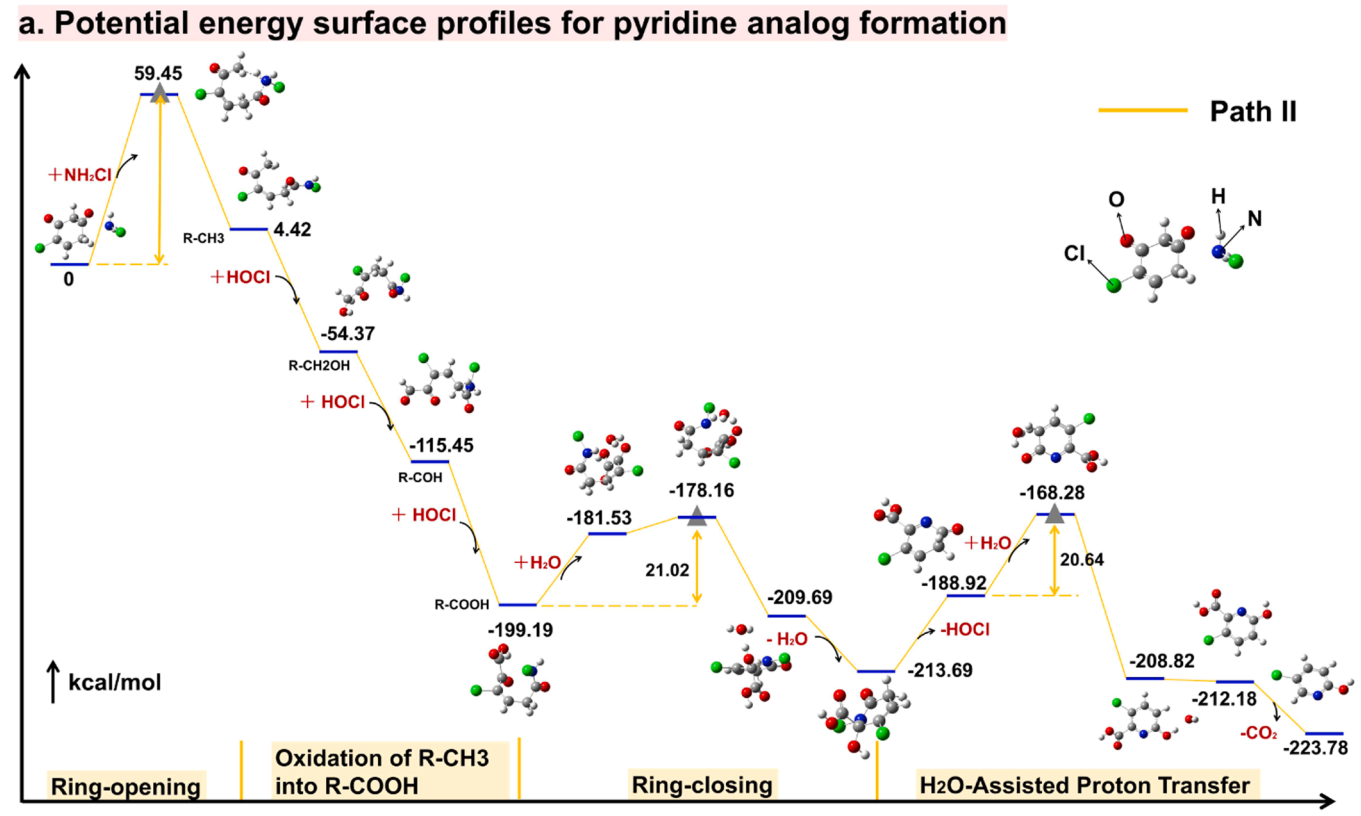

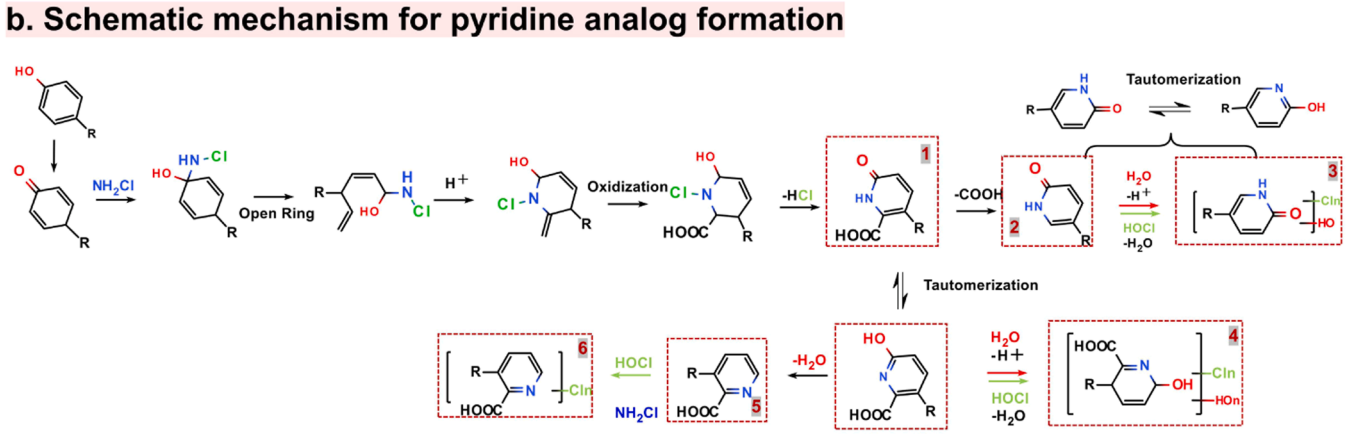

Fig. 2. (a) Profiles of the potential energy surface (Path II) and (b) schematic mechanism for pyridine analog formation. All data were calculated at the M06- 2X/def2-TZVP/IEFPCM//M06-2X/6-311G(d,p)/IEFPCM level of theory. The N-DBPs in dashed-line boxes correspond to the specific N-DBPs detected and discussed in this study.

carbon-nitrogen bond and completing the ring closure. This sequence leads to the formation of heterocyclic N-DBPs resembling pyrrole or pyridine.

To validate our proposed mechanism, we introduced theoretical calculations to gain additional mechanistic and structural insights. A general rule was introduced: for reactions of the same type, a lower $\Delta G^{\ddagger}$ value indicates greater kinetic feasibility, while a lower ΔG value suggests higher thermodynamic favorability. Thus, higher exothermicity correlates with greater thermodynamic feasibility. Considering the balance between computational cost and accuracy, we selected chlorinated N-DBPs as representative compounds for calculating halogenated N-DBPs. The potential energy surface (PES) profiles for pyridine analog formation revealed four key steps: NH_2Cl-mediated ring-opening, ring-closing rearrangement, carboxylation/decarboxylation, and H_2O-assisted proton transfer. The formation of a carboxyl group on the side chain might occur either before or after the ring-closing reaction; thus, we considered two pathways (Path I in Fig. S9 and Path II in Fig. 2(a)). Thermodynamic analysis revealed that both pathways released significant amounts of heat, indicating thermodynamic favorability. The known pathway for converting an alkane to a carboxyl group involved an initial oxidation to a hydroxyl group, conversion to an aldehyde, and finally oxidation to a carboxyl group. Given that NH_2Cl hydrolysis produced strong oxidative hypochlorous acid (HOCl), we hypothesized that HOCl mediated the formation of carboxyl groups. This HOCl-mediated carboxylation process is exothermic, indicating spontaneity and favorability ($\Delta G_{PathI} = -215$ kcal/mol; $\Delta G_{Path\ II} = -199$ kal/mol). Interestingly, forming the carboxyl group after ring-opening and then undergoing ring-closing rearrangement (Path II) helps lower the reaction's $\Delta G^{\ddagger}$ value, making the reaction more favorable ($\Delta G^{\ddagger}_{PathI} = 46.12$ kcal/mol; $\Delta G^{\ddagger}_{Path\ II} = 21.02$ kcal/mol). By comparing each reaction step, we identified that the NH_2Cl-mediated ring-opening reaction might be the rate-determining step due to its high $\Delta G^{\ddagger}$ value ($\Delta G^{\ddagger} = 59.45$ kcal/mol). Additionally, halogen substitution influences this crucial step; a higher number of chlorine substituents on quinone facilitates the ring-opening reaction ($\Delta G^{\ddagger}_{Cl=0} = 59.45$ kcal/mol; $\Delta G^{\ddagger}_{Cl=2} = 55.50$ kcal/mol; $\Delta G^{\ddagger}_{Cl=4} = 51.52$ kcal/mol). Thus, halogen substitution prior to the ring-opening reaction appears beneficial. Intrinsic reaction coordinate calculations confirmed the reaction mechanism by verifying the structures of the reactants and products of each reaction.

The PES and schematic mechanism of pyrrole analog formation (Fig. S10) revealed that the ring-closing rearrangement is the most critical step. The overall reaction is highly exothermic, indicating that the products are more stable than the reactants. Although our calculations involved high $\Delta G^{\ddagger}$ values, which might suggest alternative reaction mechanisms, the process appears thermodynamically feasible. Notably, limitations of the implicit solvation model might mean the calculated $\Delta G^{\ddagger}$ values do not fully capture solvent environment effects, potentially allowing parallel formation reactions. These findings support the proposed mechanisms for the formation of heterocyclic N-DBPs during the chloramination of phenolic compounds and emphasize the importance of halogen substitution in influencing reaction pathways. This also partly explains why 4-chlorophenol generates N-DBPs more rapidly and in larger amounts than phenol.

3.3. Identification and preliminary structure elucidation of N-DBPs from Bisphenol A as a complex phenolic precursor

Recognizing that natural organic matter (NOM) typically contains complex polyphenol structures, we expanded our study from simple phenolic precursors to more complex ones. Bisphenol A (BPA) was selected as a model compound due to its widespread environmental presence and structurally like NOM. Chloramination experiments with BPA (24-hour reaction at pH 7 with an NH_2Cl/BPA molar ratio of 10) led to the preliminary identification of over 50 novel N-DBPs through exact molecular formulas. For analysis, these N-DBPs were classified into three categories based on their carbon atom count: $C_{15}N_{1-2}X$, $C_{14}N_{1-2}X$, and $C_{13}N_{1-2}X$. Initial analysis focused on baseline N-DBPs, which are halogen-free and contain only one nitrogen atom. Molecular formulas for MS^2 fragments were obtained via database matching, while others were identified using restricted element numbers and a mass error within 20 ppm to obtain the best candidates.

Fig. S11–S14 and Figs. 3–4 present chromatographs, MS^2 fragments, and proposed structures of BPA (neg, $C_{15}H_{15}O_2$; exact mass: 227.1075; Δm = 3.8415 ppm) and its 12 baseline N-DBPs. A stable fragment ($C_9H_{11}O$ or C_9H_9O, m/z 135 or 133), consistently detected in BPA, served as a diagnostic feature having a phenolic group, indicating structural similarity between the products and BPA. The baseline N-DBPs of the $C_{15}N_{1-2}X$ category include six products ($C_{15}H_{14}NO_3$ [256a, 256b, 256c]; $C_{15}H_{14}NO_4$ [272a, 272b, 272c]). As shown in Fig. 3(a–c), 256a–c were identified as oxidation products with a carboxyl group (CO_2) at different sites. Specifically, the MS^2 fragments (Fig. 3(a–b)) of 256a and 256b ($C_{15}H_{14}NO_3$) show diagnostic fragments at m/z 133 (C_9H_9O), m/z 122 ($C_6H_4NO_2$), and m/z 78 (C_5H_4N). The m/z 133 (C_9H_9O) and m/z 122 ($C_6H_4NO_2$) are complementary to m/z 256. By comparing the m/z 122 ($C_6H_4NO_2$) and m/z 78 (C_5H_4N) fragments, it is suggested that the CO_2 group is likely located on the $C_6H_4NO_2$ moiety. For 256c, m/z 256 ($C_{15}H_{14}NO_3$) compared with m/z 212 ($C_{14}H_{14}NO$) suggests the presence of a CO_2 group. These evidences suggest that 256a–c structures may include phenolic (m/z 133, C_9H_9O), pyridine (m/z 78 (C_5H_4N) or m/z 94 (C_5H_4NO)) and CO_2 group. As shown in Fig. 3(d), the MS^2 fragments of 272a ($C_{15}H_{14}NO_4$; 272a, RT 9.9 min, Δm = 2.5882 ppm) share similarities with 256c, particularly in the fragments at m/z 185 ($C_{13}H_{13}O$) and m/z 133 (C_9H_9O), both containing carboxyl groups. Interestingly, the characteristic fragments of 272a—m/z 94 (C_5H_4NO), m/z 213 ($C_{13}H_{11}NO_2$), and m/z 228 ($C_{14}H_{14}NO_2$)—differ by 16 (one oxygen atom) from those of 256c—m/z 78 (C_5H_4N), m/z 197 ($C_{13}H_{11}NO$), and m/z 212 ($C_{14}H_{14}NO$)—suggesting that 272a may more contain a hydroxyl group than 256c or contain a C–O bond. The fragment at m/z 94 strongly indicates that the hydroxyl moiety or C–O bond is located on the pyridine ring. Similar characteristic fragments (m/z 228, m/z 133, and m/z 94) are observed for 272b, indicating similar structures with potential connectivity differences. Fig. S14(a–b) reveals diagnostic fragments and neutral losses of 272c. For example, fragments at m/z 257 ($C_{14}H_{11}NO_4$) and m/z 227 ($C_{14}H_{11}O_3$) exhibits the loss of NO moiety. Additional information from m/z 138 ($C_6H_4NO_3$) and m/z 109 ($C_6H_5O_2$) suggests co-localization of the NO moiety with another hydroxyl group (OH) on the benzene ring. Based on these structural features, we proposed that 272c consists of three OH and one NO moiety, with the NO moiety positioned on the side of the molecule containing the two HO groups.

The $C_{14}N_{1-2}X$ category includes six baseline N-DBPs observed at m/z 228, m/z 244, m/z 200, m/z 216, m/z 232, and m/z 210, as shown in Fig. 3(f), Fig. 4, and Fig. S14(c–d). Interestingly, the fragment at m/z 228 ($C_{14}H_{14}NO_2$; exact mass: 228.1022; Δm = 1.3740 ppm) resembles a fragment derived from m/z 272a–b after losing a carboxyl group, accompanied by complementary fragments at m/z 133 (C_9H_9O) and m/z 94 (C_5H_4NO). Additional structural evidence includes a neutral loss of CONH and a diagnostic phenoxy fragment (C_6H_5O). Based on this evidence, we interpreted the structure of the fragment at m/z 228 as a ketone rather than an enol. Another noteworthy finding involved a pair of decarboxylation products. The fragment at m/z 244 ($C_{14}H_{14}NO_3$; exact mass: 244.1176; Δm = –1.9921 ppm) following the loss of COOH aligned with the major fragment observed at m/z 200 ($C_{13}H_{14}NO$). Both MS^2 fragments display characteristic fragments of m/z 64 (C_4H_2N) and m/z 133 (C_9H_9O), indicating the presence of phenoxy and pyrrole rings. Additionally, as shown in Fig. 4(c–d), m/z 216 ($C_{13}H_{14}NO_2$) and m/z 232 ($C_{13}H_{14}NO_3$) are identified as consecutive hydroxylation products of m/z 200 ($C_{13}H_{14}NO$) through the interpretation of MS^2 fragments. The structure for m/z 210 ($C_{14}H_{12}NO$) is identified as a pyridine analog, supported by two neutral losses (C_2H_2) forming at m/z 183 ($C_{13}H_{11}O$), m/z 157 ($C_{11}H_9O$) and m/z 131 (C_9H_7O), with m/z 78 (C_5H_4N) characteristic of pyridine (Fig. S14(c)). Our study reveals previously

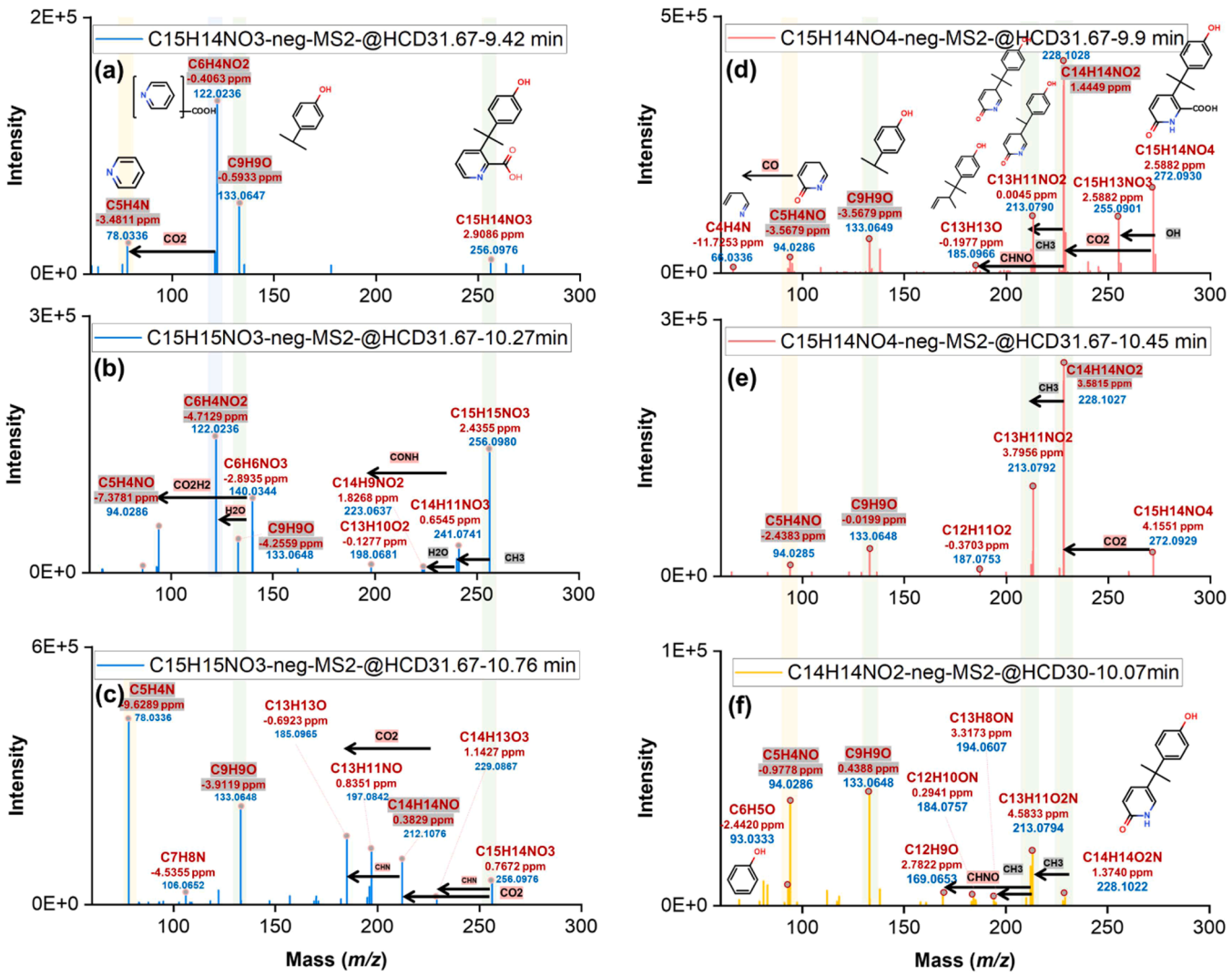

Fig. 3. MS2 spectra and proposed structures of the baseline N-DBPs (halogen-free and incorporated with only one nitrogen atom) of BPA. (a-c) m/z 256, (d-e) m/z 272, and (f) m/z 228. The MS2 fragments corresponding to those predicted by the mass frontier are shown in line. The fragments highlighted in gray represent complementary fragments. Note: The depicted structure is one of the candidate N-DBPs inferred from the molecular formula interpretation, MS2 fragments, and known or probable reactions between NH2Cl and organic chemicals.

unidentified N-DBPs of BPA, showing structural similarities to pyridine and pyrrole analogs. Some of these products also show potential for sequential chlorination, hydroxylation, and nitrogen incorporation (Fig. S15–S17). These findings suggest that the formation of heterocyclic N-DBPs during the chloramination of phenolic compounds is both feasible and likely universal, as evidenced by confirmation through commercial standards and supported by theoretical calculations.

3.4. *Unexpected formation of coupling heterocyclic N-DBPs*

Li et al. reported the formation of coupling and chlorinated coupling products during acetaminophen chlorination (Li et al., 2022). Given the partially overlapping reactivities of chloramines and chlorine, we hypothesized that chloramination might also produce coupling products. We detected both coupling and chlorinated coupling products from simple and complex phenolic precursors. For example, in BPA samples, Fig. S18(a) shows several peaks at *m/z* 453. Based on the exact molecular formula ($C_{30}H_{29}O_4$), HRMS^2 fragments, and degree of unsaturation, these peaks were identified as self-coupling DBPs of BPA, with variations in bonding patterns. Further HRMS^2 analysis (Fig. S18(b)) at *m/z* 487 revealed the formation of a monochlorinated coupling DBP ($C_{30}H_{28}ClO$; exact mass: 487.1683; Δm = 1.4841 ppm). Notably, we observed the formation of coupling N-DBPs from phenolic precursors for the first time, such as $C_{12}H_{10}NO_3$ (pos; exact mass: 216.0651; Δm = –1.8996 ppm) and $C_{12}H_9ClNO_3$ (pos; exact mass: 250.0268; Δm = 1.0492 ppm) detected in simple phenolic samples. Analysis of their MS^2 fragments indicated shared pyridine fragments (e.g., exact mass: 78.0334, C_5H_4N) with the heterocyclic N-DBPs discussed in the previous section. Similarly, peaks at *m/z* 481 ($C_{30}H_{29}N_2O_4$) and *m/z* 498 ($C_{30}H_{28}NO_6$) were observed in BPA samples. To gain more structural insight, we conducted further analysis at a higher concentration (NH_2Cl/BPA (1 mM) molar ratio of 10:1), revealing six peaks at *m/z* 498 (Fig. S19(a)). All six products contained the *m/z* 227 fragment, suggesting they might be coupling products of BPA radicals. MS^2 analysis of *m/z* 498a–c (Fig. 5 (a–b)) showed clear fragments, including the characteristic loss of CO_2. Specifically, *m/z* 498a (neutral loss C_5H_3NO) shifted from *m/z* 272 to *m/z* 320, and *m/z* 498b (neutral loss C_6H_6O) shifted from *m/z* 272 to *m/z* 319, suggesting different coupling modes with BPA. *m/z* 498a likely couples with the pyridine fraction, while *m/z* 498b likely couples with the phenol fraction. Other notable fragments include the neutral loss of CHNO in *m/z* 498a, a common fragment at *m/z* 319 ($C_{21}H_9O_3$) shared by *m/z* 498b and *m/z* 453, and a diagnostic fragment at *m/z* 94 (C_5H_4NO). Limited information on *m/z* 498c suggests a similar bonding mode to *m/z* 498a, possibly involving BPA coupling with the pyridine moiety.

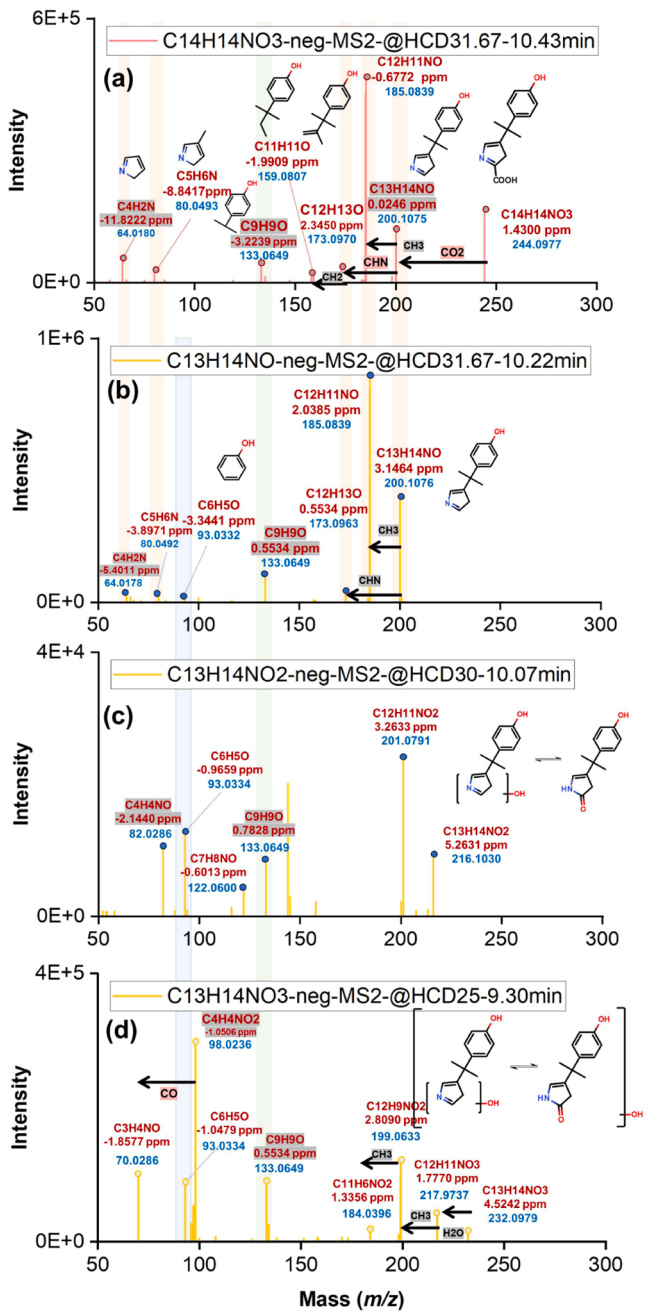

Fig. 4. MS2 spectra and proposed structures of the baseline N-DBPs (halogen-free and incorporated with only one nitrogen atom; C13-baesd and C14-based) of BPA. (a) m/z 244, (b) m/z 200, (c) m/z 216, and (d) m/z 232. The MS2 fragments corresponding to those predicted by the mass frontier are shown in line. Fragments highlighted in gray represent complementary fragments. Note: The depicted structure is one of the candidate N-DBPs inferred from the molecular formula interpretation, MS2 fragments, and known or probable reactions between NH2Cl and organic chemicals.

The absence of a complete neutral loss of CHNO suggests possible C–N bonding. We speculate that *m/z* 498a–c ($C_{30}H_{28}NO_6$) represents coupling products of BPA ($C_{15}H_{15}O_2$) with *m/z* 272 ($C_{15}H_{14}NO_4$), as shown in Fig. 5(a).

We further validated the structures and formation pathways obtained via HRMS by determining their theoretical coupling modes. Given the extensive studies on halogenated and halogen-free nitrogen-free coupling DBPs (Chen et al., 2024; Li et al., 2022; Xiang et al., 2020), we focused on the possible bonding modes of the coupling N-DBPs and choose a simple coupling product ($C_{12}H_8NO_4$) for calculations. Structurally, the bonding modes (e.g., C–C bonding) can be symmetric or antisymmetric (Fig. S20). Theoretical studies have indicated that symmetric modes are generally favored (Li et al., 2022). Therefore, our analysis concentrated on these modes, finding most of the identified coupling pathways kinetically and thermodynamically feasible (Fig. 5 (b)). Specifically, coupling through O1–C6 and O2–C4 bonds represented the most kinetically favorable pathways, with $\Delta G^{\ddagger}$ values of 2.40 and 3.87 kcal/mol, respectively, indicating rapid formation. C–C and C–O bond couplings were also kinetically favorable, with $\Delta G^{\ddagger}$ values of 7.72, 9.34, and 11.94 kcal/mol for the C4–C6, C2–C5, and C2–N bonding modes, respectively. Although C4–C6 bonds form rapidly, their products may lack the thermodynamic stability of C–N bonded products, which exhibit the highest exotherm ($\Delta G = -30$ kcal/mol). Therefore, in addition to the C–C and C–O bonded forms, the three detectable *m/z* 487 peaks likely include C–N coupling DBPs (Fig. 5(c)), which were cross-validated using $HRMS^2$. Although other bonding modes may exist, the major fragments fit the hypothesized structure well, and the theoretically calculated bonding modes support this interpretation. While the occurrence of BPA or phenol radical coupling may be rare at low concentrations, it is crucial to recognize this coupling pattern, given the abundant phenolic structures in NOM and the potential toxicity of these coupling heterocyclic N-DBPs. Additionally, the MS^2 fragments of three additional structures at *m/z* 498 (Fig. S19(b)) revealed neutral losses of NO and NO_2 as well as fragments shared with the self-coupling product at *m/z* 453. These DBPs likely represent self-coupling products involving nitro/nitroso substitutions.

3.5. Selective formation of N-DBPs under varying chloramination conditions

Complex phenolic compounds can generate a wider range of N-DBPs, making them more responsive to varying disinfection conditions. In this section, BPA was chosen to examine how different disinfection conditions affect N-DBP formation. For clarity, N-DBPs were classified into C13-based, C14-based, and C15-based categories. Due to the lack of standards, the relative concentrations of each DBP or DBP class were estimated using peak areas obtained through selected ion monitoring

3.5.1. Effect of reaction time, monochloramine dosage and pH

After 12 hours of reaction (at an NH_2Cl/BPA molar ratio of 10:1 and pH 7), halogenated N-DBPs and those with more than two nitrogen atoms (N_2-DBPs) began to accumulate (Fig. S21), indicating partial conversion of baseline N-DBPs into more complex forms. Assuming that the peak areas of structurally similar products are proportional to their concentrations, all novel N-DBPs continued to accumulate over 48 hours, indicating their relative persistence.

The impact of NH_2Cl dosage on N-DBP formation was investigated by varying the NH_2Cl/BPA molar ratios (5, 10, 20, and 50). As the NH_2Cl/BPA molar ratio increased from 5 to 50, the BPA conversion increased from 30 % to 100 % (Fig. S22). Although NH_2Cl was present in excess relative to BPA (Fig. S23), N-DBPs steadily accumulating over 48 hours, indicating a preference for BPA conversion to N-DBPs at higher NH_2Cl dosages (Fig. 6). Higher NH_2Cl dosages also favored the formation of halogenated N-DBPs and N_2-DBPs, while the significance of baseline N-DBPs decreased at a 50:1 NH_2Cl/BPA ratio. Over the 48-hour period, N-DBPs yields initially increased and then decreased, shifting toward chlorination and the formation of N_2-DBPs. This suggests that NH_2Cl dosage influences both chlorine substitution and nitrogen incorporation, and these processes may also benefit from HOCl, as higher NH_2Cl concentrations could hydrolyze to release more HOCl. Notably, the formation of coupling DBPs differed from that of heterocyclic N-DBPs, which depended on electron transfer reactions with chlorine. Accumulation decreased when the NH_2Cl/BPA ratio exceeded 20:1, indicating that higher NH_2Cl doses more likely promote BPA conversion to heterocyclic N-DBPs rather than coupling DBPs. pH also significantly affected N-

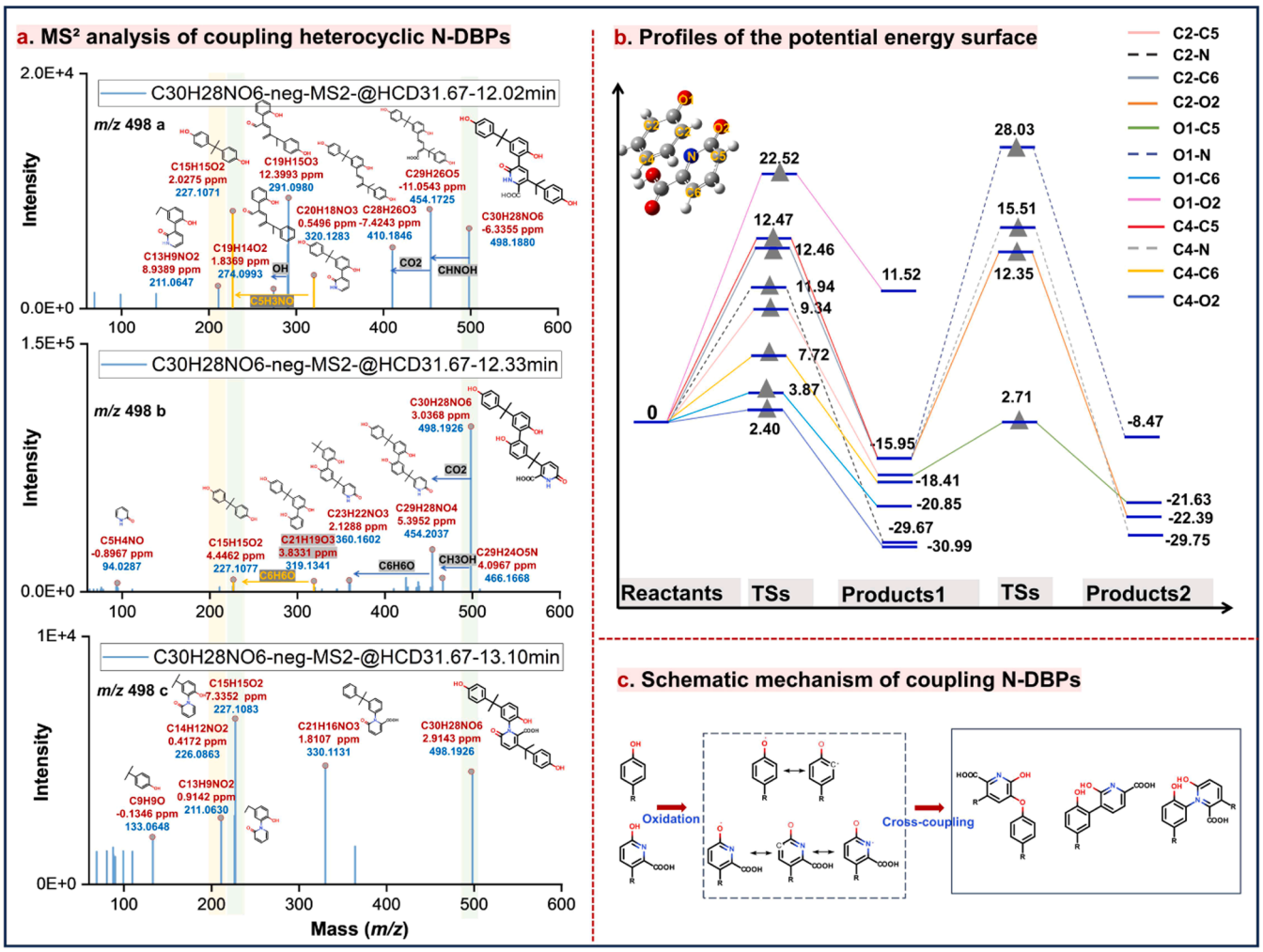

Fig. 5. (a) MS2 spectra, (b) the possible bonding modes, and (c) schematic mechanism of m/z 498 formation. All the data were calculated at the M06-2X/def2-TZVP/IEFPCM//M06-2X/6-311G(d,p)/IEFPCM level of theory. Note: The depicted structure is one of the candidate N-DBPs inferred from the molecular formula interpretation, MS2 fragments, and known or probable reactions between NH2Cl and organic chemicals.

DBPs formation. As shown in Fig. S24, chloramination experiments was conducted over a pH range of 4–10. revealed that BPA conversion was hindered under highly acidic and basic conditions, particularly for N-DBPs. In contrast, N-DBPs formation was significantly higher in the pH range 6–8. This trend may be attributed to the reactivity of halobenzoquinone (HBQ), a key intermediate in the conversion pathway. Previous studies have demonstrated that the reaction between hypochlorite and HBQs is strongly pH-dependent, with reactivity increasing and then decreasing within the pH rang 5–10 (Gao et al., 2024). Given the similarities between chlorination and chloramination, we hypothesized that a similar phenomenon would occur. However, coupling DBPs exhibited a different pattern, with alkaline conditions favoring accumulation over acidic conditions, likely due to the increased role of phenoxy radical intermediates in coupling DBP formation.

3.5.2. *Effect of NOM and alkalinity*

In natural water, NOM is widely present and can interact or compete with other components during chloramination. As shown in Fig. S25, the presence of NOM (3 mg-C/L) slightly inhibited the formation of N-DBPs. This inhibition is likely due to phenolic or polyphenolic compounds in NOM, which effectively consume chloramines. We also evaluated the effect of alkalinity on N-DBP formation. As shown in Fig. S26, the presence of bicarbonate (HCO_3^-, 2 mM) slightly reduced the concentration of N-DBPs, likely due to bicarbonate acting as a radical scavenger and inhibiting N-DBP formation by reacting with radical intermediates.

3.5.3. *Effect of bromide*

Bromide, commonly found in source water, was tested at varying concentrations (0–20 μM). As shown in Fig. 7, fourteen newly brominated N-DBPs were identified in the bromide-containing samples. Bromide presence significantly reduced the accumulation of non-brominated heterocyclic N-DBPs, while concurrently promoting the formation of brominated heterocyclic N-DBPs. This can be explained by the reaction of bromide with NH_2Cl to form bromoamines, which exhibited higher reactivity with BPA than with NH_2Cl. Brominated N-DBPs were formed through two pathways: incorporation of bromine-bromoamines into BPA or bromine substitution of N-DBP. Interestingly, Fig. 7(d) shows that bromide significantly inhibited the formation of coupling DBPs, decreasing with increasing bromide concentration, which was in contrast with the observations in chlorination (Li et al., 2022). Specifically, bromide reacted with NH_2Cl favor bromoamines formation over HOBr, whereas the formation of coupling DBPs primarily relied on electron transfer from HOBr. Unlike heterocyclic N-DBPs, brominated coupling DBPs were not detected, possibly because bromide catalyzed the electron transfer process rather than engaging in bromophilic reactions (Criquet et al., 2015). Additionally, steric hindrance may also play a role, as the formation of coupling N-DBPs involves radical intermediates, and bulky substituents like bromine atom increase steric requirements, making it more difficult for radical intermediates to couple effectively, thus inhibiting the formation of brominated coupling N-DBPs.

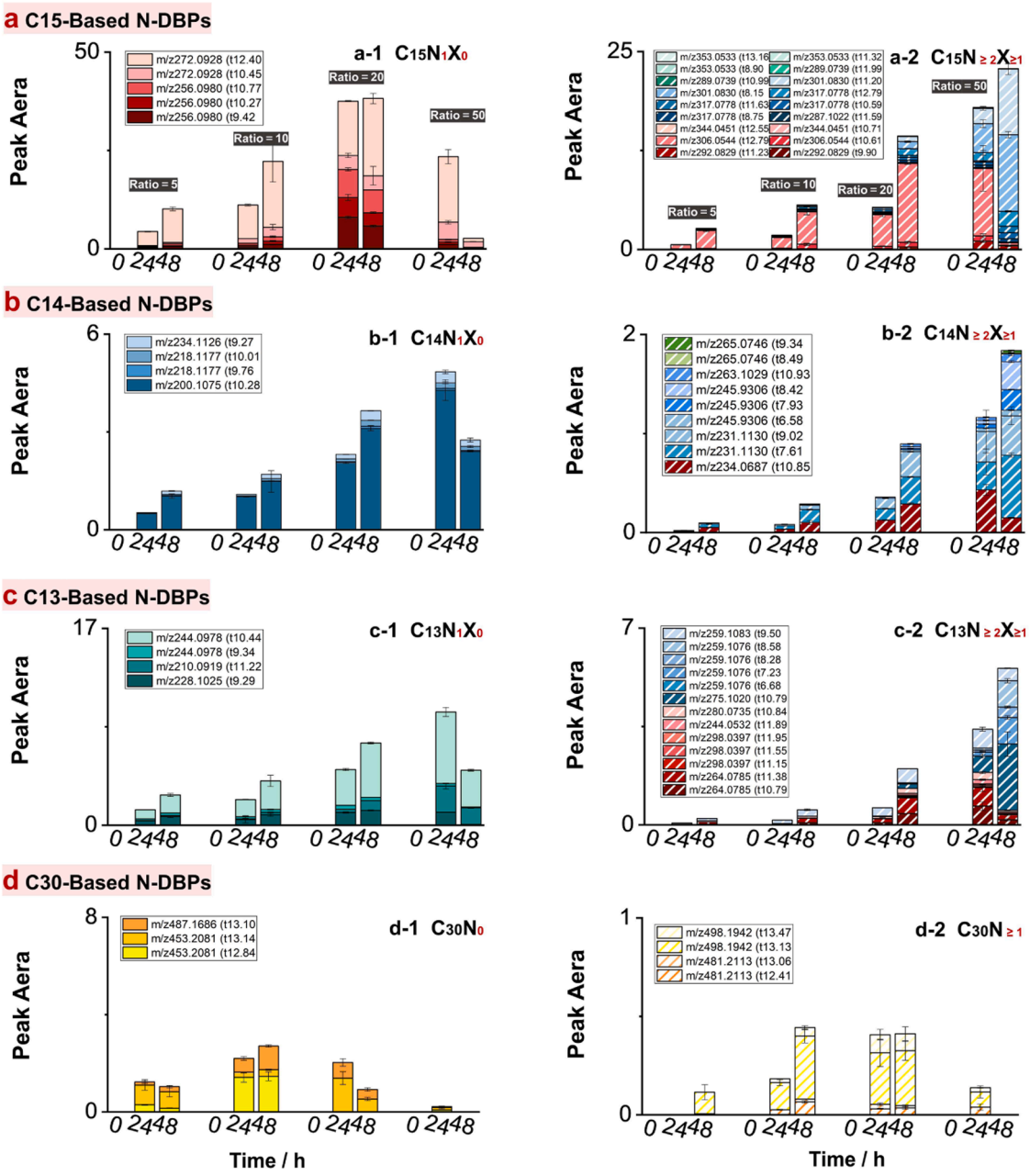

Fig. 6. Formation of four groups of N-DBPs at different NH2Cl doses and NH2Cl/BPA molar ratios of 5–50: (a) C15-based DBPs, (b) C14-based DBPs, (c) C13-based DBPs, and (d) C30-based DBPs. Reaction conditions: [NH2Cl]0 = 50–500 μM, [BPA]0 = 10 μM, T = 23 ± 2°C, [phosphate buffer] = 5.0 mM, pH = 7 ± 0.2. Solid colors represent baseline (halogen-free and incorporated with only one nitrogen atom) N-DBPs; red slashes express halogenated N-DBPs; blue slashes represent N-DBPs with N≥2; and green slashes represent halogenated N-DBPs with N≥2.

3.6. Verification of novel N-DBP formation under environmentally relevant conditions

We further investigated the formation of those N-DBPs under environmentally relevant conditions, using realistic concentrations of model compounds and NH_2Cl. Chloramination was conducted with 1 mg/L NH_2Cl over 24 hours, starting with initial BPA concentrations of 0.1 μM and simple phenolic compounds (phenol, 4-chlorophenol, 4-bromophenol) at 0.02 μM. As shown in Fig. S27–S28, most N-DBPs identified in high-concentration samples were also detected in low-concentration samples, confirming the widespread formation of these N-DBPs during the chloramination of phenolic compounds. These findings underscore the potential for N-DBP formation across a range of environmental conditions, suggesting that these N-DBPs may be more common in treated water supplies than previously thought. Given the large number and diversity of phenolic compounds, their potential role as precursors to heterocyclic N-DBPs during disinfection should not be overlooked.

4. Conclusions

In this study, we report for the first time that chloramination of phenolic compounds leads to the formation of nearly 100 novel HWM N-DBPs. We provide novel insights into their structures and formation mechanisms from both computational and experimental perspectives. The main conclusions are summarized as follows:

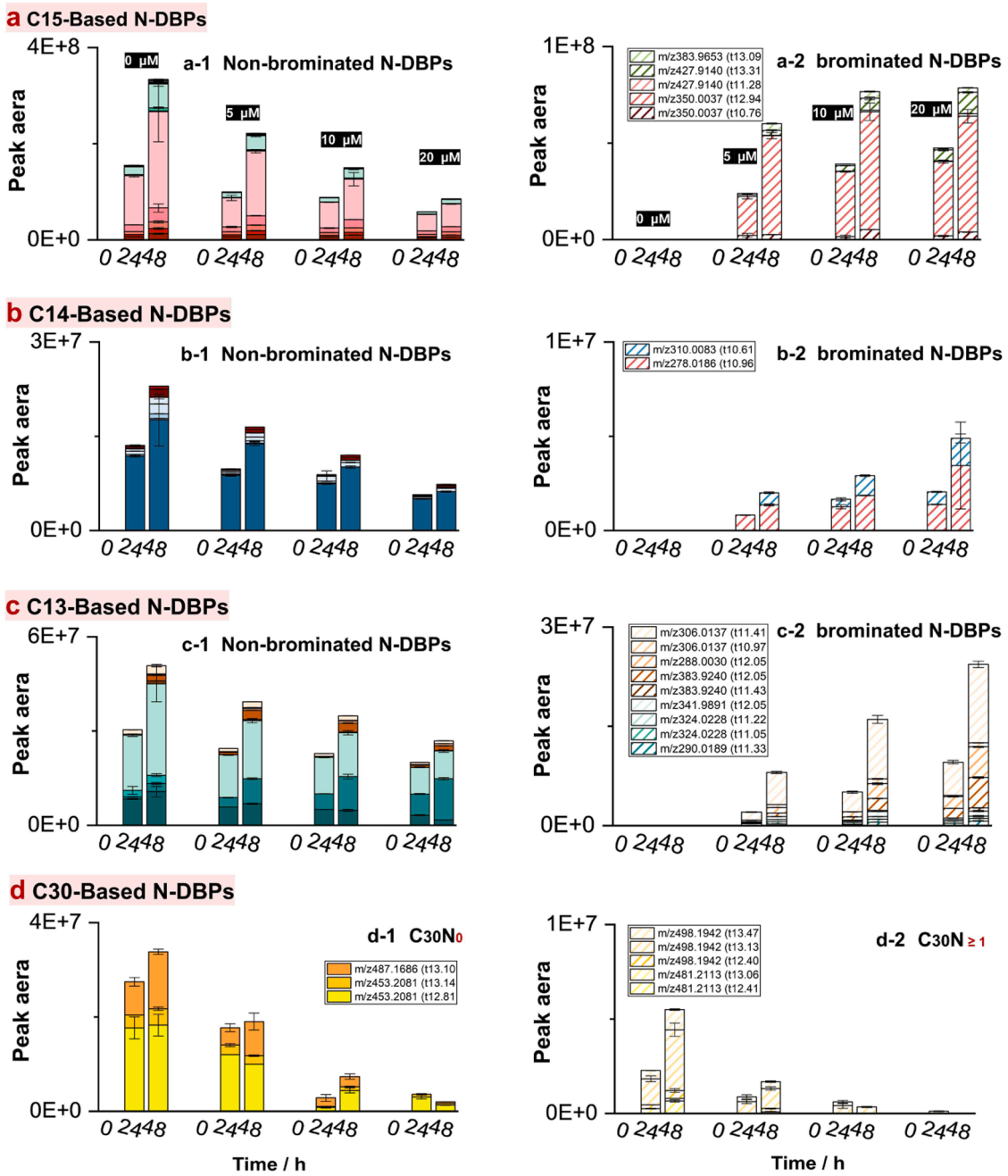

Fig. 7. Formation of four groups of N-DBPs at different initial bromide concentrations: (a) C15-based N-DBPs, (b) C14-based N-DBPs, (c) C13-based N-DBPs, and (d) C30- based N-DBPs. Reaction conditions: [NH2Cl]0 = 100 μM, [Br–]0 = 0–20 μM, [BPA]0 = 10 μM, T = 23 ± 2°C, [phosphate buffer] = 5.0 mM, pH = 7 ± 0.2. Solid colors represent non-brominated N-DBPs, and slashes represent newly brominated N-DBPs.

1. Novel HWM N-DBPs, initially identified as heterocyclic and coupling heterocyclic N-DBPs, form during the chloramination of phenolic compounds.
2. Those novel N-DBPs can form at environmentally relevant levels of phenolic precursors and monochloramine dosage.
3. The key step in the formation of heterocyclic N-DBPs is the ring-opening reaction between halobenzoquinones and NH_2Cl. The coupling heterocyclic N-DBPs involve new preferred bonding modes (C–N, C–O, and C–C bonding), as confirmed by HRMS and DFT calculations
4. Formation of novel N-DBPs is significantly influenced by NH_2Cl dosage, pH, and contact time. Higher NH_2Cl dosage facilitates the formation of chlorinated N-DBPs and N-DBPs with more than one nitrogen atom.
5. Bromide promotes the formation of brominated heterocyclic N-DBPs; brominated coupling N-DBPs were not detected.

CRediT authorship contribution statement

Pin Wang: Writing – review & editing, Writing – original draft, Visualization, Software, Methodology, Formal analysis, Data curation. **Bei Ye:** Writing – review & editing, Visualization, Validation, Conceptualization. **Youhei Nomura:** Writing – review & editing, Visualization, Validation, Methodology. **Taku Fujiwara:** Writing – review & editing, Supervision, Resources, Project administration, Data curation, Conceptualization.

Declaration of competing interest

The authors declare that they have no known competing financial interests or personal relationships that could have appeared to influence the work reported in this paper.

Data availability

Data will be made available on request.

Acknowledgements

This research used the supercomputer system of Academic Center for Computing and Media Studies, Kyoto University. We extend our appreciation to the staffs for their unwavering support and dedication throughout our research activities. We would like to express our gratitude to Dr. Zijiang Yang (Tokyo University of Marine Science and Technology) and Dr. Klon D.C. Hinneh (Kyoto University) for their insightful discussions. We thank Dr. Shinya Echigo (Kyoto University) for his beneficial suggestions and discussions on the mass spectrometry analysis. We would like to thank Editage (www.editage.jp) for English language editing.

Supplementary materials

Supplementary material associated with this article can be found, in the online version, at doi:10.1016/j.watres.2024.122335.

References

Aeschbacher, M., Graf, C., Schwarzenbach, R.P., Sander, M., 2012. Antioxidant Properties of Humic Substances. Environ. Sci. Technol. 46, 4916–4925. https://doi.org/10.1021/es300039h.

Angeles, L.F., Singh, R.R., Vikesland, P.J., Aga, D.S., 2021. Increased coverage and high confidence in suspect screening of emerging contaminants in global environmental samples. J. Hazard. Mater. 414, 125369 https://doi.org/10.1016/j.jhazmat.2021.125369.

Awwa Disinfection Systems Committee, 2008. Committee Report: Disinfection Survey, Part2—Alternatives, experiences, and future plans. J. Am. Water Works Assoc. 100, 110–124. https://doi.org/10.1002/j.1551-8833.2008.tb09778.x.

Chen, Y., Liang, Q., Liang, W., Li, W., Liu, Y., Guo, K., Yang, B., Zhao, X., Yang, M., 2023. Identification of toxicity forcing agents from individual aliphatic and aromatic disinfection byproducts formed in drinking water: implications and limitations. Environ. Sci. Technol. 57, 1366–1377. https://doi.org/10.1021/acs.est.2c07629.

Chen, Y., Ren, W., Ma, T., Ren, N., Wang, S., Duan, X., 2024. Transformative removal of aqueous micropollutants into polymeric products by advanced oxidation processes. Environ. Sci. Technol. 58, 4844–4851. https://doi.org/10.1021/acs.est.3c06376.

Chen, Z., Chen, J., Tan, S., Yang, Z., Zhang, Y., 2024. Dechlorination helps defluorination: insights into the defluorination mechanism of florfenicol by s-nzvi and dft calculations on the reaction pathways. Environ. Sci. Technol. 58, 2542–2553. https://doi.org/10.1021/acs.est.3c07435.

Criquet, J., Rodriguez, E.M., Allard, S., Wellauer, S., Salhi, E., Joll, C.A., von Gunten, U., 2015. Reaction of bromine and chlorine with phenolic compounds and natural organic matter extracts – Electrophilic aromatic substitution and oxidation. Water Res 85, 476–486. https://doi.org/10.1016/j.watres.2015.08.051.

Dualde, P., Miralles, P., Peris-Martínez, C., Yusà, V., Coscollà, C., 2023. Untargeted analysis and tentative identification of unknown substances in human tears by ultra-high performance liquid chromatography-high resolution mass spectrometry: Pilot study. J. Chromatogr. B 1228, 123832. https://doi.org/10.1016/j.jchromb.2023.123832.

Fiss, E.M., Rule, K.L., Vikesland, P.J., 2007. Formation of chloroform and other chlorinated byproducts by chlorination of triclosan-containing antibacterial products. Environ. Sci. Technol. 41, 2387–2394. https://doi.org/10.1021/es062227l.

Gao, X., Wang, X., Jiang, Y., Kong, D., Pan, X., Ma, J., Liu, Y., 2024. Chloro- and bromo-benzoquinone formation and transformation mechanisms in a drinking water-distribution system. J. Hazard. Mater. 461, 132692 https://doi.org/10.1016/j.jhazmat.2023.132692.

Hoigné, J., Bader, H., 1988. The formation of trichloronitromethane (chloropicrin) and chloroform in a combined ozonation/chlorination treatment of drinking water. Water Res 22, 313–319. https://doi.org/10.1016/S0043-1354(88)90120-0.

Hu, S., Chen, X., Zhang, B., Liu, L., Gong, T., Xian, Q., 2022. Occurrence and transformation of newly discovered 2-bromo-6-chloro-1,4-benzoquinone in chlorinated drinking water. J. Hazard. Mater. 436, 129189 https://doi.org/10.1016/j.jhazmat.2022.129189.

Jeon, J., Kurth, D., Hollender, J., 2013. Biotransformation pathways of biocides and pharmaceuticals in freshwater crustaceans based on structure elucidation of metabolites using high resolution mass spectrometry. Chem. Res. Toxicol. 26, 313–324. https://doi.org/10.1021/tx300457f.

Joo, S.H., Mitch, W.A., 2007. Nitrile, Aldehyde, and Halonitroalkane formation during chlorination/chloramination of primary amines. Environ. Sci. Technol. 41, 1288–1296. https://doi.org/10.1021/es0612697.

Kirmeyer, G.J., 2004. Optimizing chloramine treatment. American Water Works Association.

Kosaka, K., Nakai, T., Hishida, Y., Asami, M., Ohkubo, K., Akiba, M., 2017. Formation of 2,6-dichloro-1,4-benzoquinone from aromatic compounds after chlorination. Water Res 110, 48–55. https://doi.org/10.1016/j.watres.2016.12.005.

Lau, S.S., Bokenkamp, K., Tecza, A., Wagner, E.D., Plewa, M.J., Mitch, W.A., 2023. Toxicological assessment of potable reuse and conventional drinking waters. Nat. Sustain. 6, 39–46. https://doi.org/10.1038/s41893-022-00985-7.

Li, J., Aziz, Md.T., Granger, C.O., Richardson, S.D., 2021. Are Disinfection Byproducts (DBPs) Formed in My Cup of Tea? Regulated, Priority, and Unknown DBPs. Environ. Sci. Technol. 55, 12994–13004. https://doi.org/10.1021/acs.est.1c03419.

Li, W., Zhang, X., Han, J., 2022. Formation of larger molecular weight disinfection byproducts from acetaminophen in chlorine disinfection. Environ. Sci. Technol. 56, 16929–16939. https://doi.org/10.1021/acs.est.2c06394.

Li, X.-F., Mitch, W.A., 2018. Drinking water disinfection byproducts (dbps) and human health effects: multidisciplinary challenges and opportunities. Environ. Sci. Technol. 52, 1681–1689. https://doi.org/10.1021/acs.est.7b05440.

Liljenberg, M., Stenlid, J.H., Brinck, T., 2018. Theoretical investigation into rate-determining factors in electrophilic aromatic halogenation. J. Phys. Chem. A 122, 3270–3279. https://doi.org/10.1021/acs.jpca.7b10781.

Lu, Y., Song, Z.-M., Wang, C., Liang, J.-K., Xu, N., Hu, Q., Wu, Q.-Y., 2021. Combination of high resolution mass spectrometry and a halogen extraction code to identify chlorinated disinfection byproducts formed from aromatic amino acids. Water Res 190, 116710. https://doi.org/10.1016/j.watres.2020.116710.

Mitch, W.A., Richardson, S.D., Zhang, X., Gonsior, M., 2023. High-molecular-weight by-products of chlorine disinfection. Nat. Water 1, 336–347. https://doi.org/10.1038/s44221-023-00064-x.

Muellner, M.G., Wagner, E.D., McCalla, K., Richardson, S.D., Woo, Y.-T., Plewa, M.J., 2007. Haloacetonitriles vs. Regulated Haloacetic Acids: Are Nitrogen-Containing DBPs More Toxic? Environ. Sci. Technol. 41, 645–651. https://doi.org/10.1021/es0617441.

Nihemaiti, M., Icker, M., Seiwert, B., Reemtsma, T., 2023. Revisiting disinfection byproducts with supercritical fluid chromatography-high resolution-mass spectrometry: identification of novel halogenated sulfonic acids in disinfected drinking water. Environ. Sci. Technol. 57, 3527–3537. https://doi.org/10.1021/acs.est.2c05536.

Nihemaiti, M., Le Roux, J., Hoppe-Jones, C., Reckhow, D.A., Croué, J.-P., 2017. Formation of Haloacetonitriles, Haloacetamides, and Nitrogenous Heterocyclic Byproducts by Chloramination of Phenolic Compounds. Environ. Sci. Technol. 51, 655–663. https://doi.org/10.1021/acs.est.6b04819.

Pan, W., Zhang, D., Han, Z., Zhan, J., Liu, C., 2013. New Insight into the Formation Mechanism of PCDD/Fs from 2-Chlorophenol Precursor. Environ. Sci. Technol. 47, 8489–8498. https://doi.org/10.1021/es400632j.

Pan, Y., Wang, Y., Li, A., Xu, B., Xian, Q., Shuang, C., Shi, P., Zhou, Q., 2017. Detection, formation and occurrence of 13 new polar phenolic chlorinated and brominated disinfection byproducts in drinking water. Water Res 112, 129–136. https://doi.org/10.1016/j.watres.2017.01.037.

Pan, Y., Zhang, X., 2013. Four groups of new aromatic halogenated disinfection byproducts: effect of bromide concentration on their formation and speciation in chlorinated drinking water. Environ. Sci. Technol. 47, 1265–1273. https://doi.org/10.1021/es303729n.

Plewa, M.J., Muellner, M.G., Richardson, S.D., Fasano, F., Buettner, K.M., Woo, Y.-T., McKague, A.B., Wagner, E.D., 2008. Occurrence, synthesis, and mammalian cell cytotoxicity and genotoxicity of haloacetamides: an emerging class of nitrogenous drinking water disinfection byproducts. Environ. Sci. Technol. 42, 955–961. https://doi.org/10.1021/es071754h.

Plewa, M.J., Simmons, J.E., Richardson, S.D., Wagner, E.D., 2010. Mammalian cell cytotoxicity and genotoxicity of the haloacetic acids, a major class of drinking water disinfection by-products. Environ. Mol. Mutagen. 51, 871–878. https://doi.org/10.1002/em.20585.

Plewa, M.J., Wagner, E.D., Jazwierska, P., Richardson, S.D., Chen, P.H., McKague, A.B., 2004. Halonitromethane drinking water disinfection byproducts: chemical characterization and mammalian cell cytotoxicity and genotoxicity. Environ. Sci. Technol. 38, 62–68. https://doi.org/10.1021/es030477l.

Prasse, C., von Gunten, U., Sedlak, D.L., 2020. Chlorination of Phenols Revisited: Unexpected Formation of α,β-Unsaturated C4-Dicarbonyl Ring Cleavage Products. Environ. Sci. Technol. 54, 826–834. https://doi.org/10.1021/acs.est.9b04926.

Richardson, S.D., Ternes, T.A., 2018. Water analysis: emerging contaminants and current issues. Anal. Chem. 90, 398–428. https://doi.org/10.1021/acs.analchem.7b04577.

Schreiber, I.M., Mitch, W.A., 2005. Influence of the Order of Reagent Addition on NDMA Formation during Chloramination. Environ. Sci. Technol. 39, 3811–3818. https://doi.org/10.1021/es0483286.

Seidel, C.J., McGuire, M.J., Summers, R.S., Via, S., 2005. Have utilities switched to chloramines? J. AWWA 97, 87–97. https://doi.org/10.1002/j.1551-8833.2005.tb07497.x.

Shah, A.D., Mitch, W.A., 2012. Halonitroalkanes, Halonitriles, Haloamides, and N-Nitrosamines: A Critical Review of Nitrogenous Disinfection Byproduct Formation Pathways. Environ. Sci. Technol. 46, 119–131. https://doi.org/10.1021/es203312s.

Sun, X., Wei, D., Wang, F., Yang, F., Du, Y., Xiao, H., Wei, X., Xiao, A., 2024. Formation of nitrogen-containing disinfection by-products during the chloramination treatment of an emerging pollutant. Chemosphere 353, 141536. https://doi.org/10.1016/j.chemosphere.2024.141536.

Tang, H., Zhong, H., Pan, Y., Zhou, Q., Huo, Z., Chu, W., Xu, B., 2021. A New group of heterocyclic nitrogenous disinfection byproducts (DBPs) in drinking water: role of extraction pH in Unknown DBP Exploration. Environ. Sci. Technol. 55, 6764–6772. https://doi.org/10.1021/acs.est.1c00078.

Tentscher, P.R., Bourgin, M., von Gunten, U., 2018. Ozonation of Para-Substituted Phenolic Compounds Yields p-Benzoquinones, Other Cyclic α,β-Unsaturated Ketones, and Substituted Catechols. Environ. Sci. Technol. 52, 4763–4773. https://doi.org/10.1021/acs.est.8b00011.

Valentine, R.L., Brandt, K.I., Jafvert, C.T., 1986. A spectrophotometric study of the formation of an unidentified monochloramine decomposition product. Water Res 20, 1067–1074. https://doi.org/10.1016/0043-1354(86)90051-5.

Wang, W., Qian, Y., Boyd, J.M., Wu, M., Hrudey, S.E., Li, X.-F., 2013. Halobenzoquinones in Swimming Pool Waters and Their Formation from Personal Care Products. Environ. Sci. Technol. 47, 3275–3282. https://doi.org/10.1021/es304938x.

Wang, Y., Vorsa, N., Harrington, P., de, B., Chen, P., 2018. Nontargeted Metabolomic Study on Variation of Phenolics in Different Cranberry Cultivars Using UPLC-IM – HRMS. J. Agric. Food Chem. 66, 12206–12216. https://doi.org/10.1021/acs.jafc.8b05029.

Wendel, F.M., Lütke Eversloh, C., Machek, E.J., Duirk, S.E., Plewa, M.J., Richardson, S. D., Ternes, T.A., 2014. Transformation of Iopamidol during Chlorination. Environ. Sci. Technol. 48, 12689–12697. https://doi.org/10.1021/es503609s.

Xiang, W., Qu, R., Wang, X., Wang, Z., Bin-Jumah, M., Allam, A.A., Zhu, F., Huo, Z., 2020. Removal of 4-chlorophenol, bisphenol A and nonylphenol mixtures by aqueous chlorination and formation of coupling products. Chem. Eng. J. 402, 126140 https://doi.org/10.1016/j.cej.2020.126140.

Yamamoto, T., Yasuhara, A., 2002. Chlorination of bisphenol A in aqueous media: formation of chlorinated bisphenol A congeners and degradation to chlorinated phenolic compounds. Chemosphere 46, 1215–1223. https://doi.org/10.1016/S0045-6535(01)00198-9.

Yang, J., Li, W., Zhu, Q., Yang, M., Li, J., Zhang, J., Yang, B., Zhao, X., 2019. Identification, formation, and predicted toxicity of halogenated dbps derived from tannic acid and its biodegradation products. Environ. Sci. Technol. 53, 13019–13030. https://doi.org/10.1021/acs.est.9b03073.

Yang, M., Zhang, X., 2013. Comparative Developmental Toxicity of New Aromatic Halogenated DBPs in a Chlorinated Saline Sewage Effluent to the Marine Polychaete Platynereis dumerilii. Environ. Sci. Technol. 47, 10868–10876. https://doi.org/10.1021/es401841t.

Yu, H., Kiley, K., Kullar, S., Fu, K., Tran, T.N., Wang, H., Hu, J., Kamberi, M., 2023. A Chemical characterization workflow for nontargeted analysis of complex extracts from polymer based medical device using high resolution LC/MS. ACS Biomater. Sci. Eng. 9, 2277–2291. https://doi.org/10.1021/acsbiomaterials.2c01467.

Zhai, H., Zhang, X., 2011. Formation and Decomposition of new and unknown polar brominated disinfection byproducts during chlorination. Environ. Sci. Technol. 45, 2194–2201. https://doi.org/10.1021/es1034427.

Zhang, C., Chen, B., Korshin, G.V., Kuznetsov, A.M., Roccaro, P., Yan, M., Ni, J., 2020. Comparison of the yields of mono-, Di- and tri-chlorinated HAAs and THMs in chlorination and chloramination based on experimental and quantum-chemical data. Water Res 169, 115100. https://doi.org/10.1016/j.watres.2019.115100.

Zhang, D., Bond, T., Li, M., Dong, S., Pan, Y., Du, E., Xiao, R., Chu, W., 2021. Ozonation Treatment Increases Chlorophenylacetonitrile Formation in Downstream Chlorination or Chloramination. Environ. Sci. Technol. 55, 3747–3755. https://doi.org/10.1021/acs.est.0c07853.

Zhang, D., Bond, T., Pan, Y., Li, M., Luo, J., Xiao, R., Chu, W., 2022. Identification, Occurrence, and Cytotoxicity of Haloanilines: A New Class of Aromatic Nitrogenous Disinfection Byproducts in Chloraminated and Chlorinated Drinking Water. Environ. Sci. Technol. 56, 4132–4141. https://doi.org/10.1021/acs.est.1c07375.

Zhang, D., Chu, W., Yu, Y., Krasner, S.W., Pan, Y., Shi, J., Yin, D., Gao, N., 2018. Occurrence and Stability of Chlorophenylacetonitriles: A New Class of Nitrogenous Aromatic DBPs in Chlorinated and Chloraminated Drinking Waters. Environ. Sci. Technol. Lett. 5, 394–399. https://doi.org/10.1021/acs.estlett.8b00220.

Zhang, W., Zhong, J., Shi, Q., Gao, L., Ji, Y., Li, G., An, T., Francisco, J.S., 2021. Mechanism for Rapid Conversion of Amines to Ammonium Salts at the Air–Particle Interface. J. Am. Chem. Soc. 143, 1171–1178. https://doi.org/10.1021/jacs.0c12207.

Zhang, Y., Liu, J., Moores, A., Ghoshal, S., 2020. Transformation of 6:2 Fluorotelomer Sulfonate by Cobalt(II)-Activated Peroxymonosulfate. Environ. Sci. Technol. 54, 4631–4640. https://doi.org/10.1021/acs.est.9b07113.

Zhao, Y., Anichina, J., Lu, X., Bull, R.J., Krasner, S.W., Hrudey, S.E., Li, X.-F., 2012. Occurrence and formation of chloro- and bromo-benzoquinones during drinking water disinfection. Water Res. 46, 4351–4360. https://doi.org/10.1016/j.watres.2012.05.032.

Zhou, Y., Jiao, J., Huang, H., Liu, Y.D., Zhong, R., Yang, X., 2023. Insights into C–C Bond cleavage mechanisms in dichloroacetonitrile formation during Chlorination of Long-chain primary amines, amino acids, and dipeptides. Environ. Sci. Technol. 57, 18834–18845. https://doi.org/10.1021/acs.est.2c07779.